Geophysical Research Letters

RESEARCH LETTER
10.1029/2022GL101704

Structure and Dynamics of Lithosphere and Asthenosphere in Asia: A Seismological Perspective

Jincheng Ma[1], Hans-Peter Bunge[1], Andreas Fichtner[2], Sung-Joon Chang[3], and You Tian[4]

[1]Department of Earth and Environmental Sciences, Ludwig-Maximilians-Universität München, Munich, Germany, [2]Department of Earth Sciences, ETH Zürich, Zurich, Switzerland, [3]Department of Geophysics, Kangwon National University, Chuncheon, South Korea, [4]College of Geoexploration Science and Technology, Jilin University, Changchun, China

Key Points:

- Full-waveform tomographic images reveal lateral heterogeneities and anisotropy in the lithosphere and asthenosphere beneath the Asian region
- India-Eurasia collision induced large-scale low-velocity anomaly and crustal thickening spanning from the Himalayas to the Baikal rift zone
- Asthenosphere in East and SE Asia exhibits strong v_{sh}, > v_{sv}, and partially decouples lithosphere, bounded by subduction trench and cratonic keels

Supporting Information:

Supporting Information may be found in the online version of this article.

Correspondence to:

J. Ma,
jincheng.ma@geophysik.uni-muenchen.de

Citation:

Ma, J., Bunge, H.-P., Fichtner, A., Chang, S.-J., & Tian, Y. (2023). Structure and dynamics of lithosphere and asthenosphere in Asia: A seismological perspective. *Geophysical Research Letters*, *50*, e2022GL101704. https://doi.org/10.1029/2022GL101704

Received 21 NOV 2022
Accepted 8 FEB 2023

Abstract Knowledge of lithospheric structure is essential for understanding the impact of continental collision and oceanic subduction on surface tectonic configurations. Full-waveform tomographic images reveal lateral heterogeneities and anisotropy of the lithosphere and asthenosphere in Asia. Estimating lithospheric thickness from seismic velocity reductions at depth exhibits large variations underneath different tectonic units. The thickest cratonic roots are present beneath the Sichuan, Ordos, and Tarim basins and central India. Radial anisotropy signatures of 11 representative tectonic provinces uncover the different nature and geodynamic processes of their respective past and present deformation. The large-scale continental lithospheric deformation is characterized by low-velocity anomalies from the Himalayan Orogen to the Baikal rift zone in central Asia, coupled with the post-collision thickening of the crust. The horizontal low-velocity layer of ∼100–300 km depth extent below the lithosphere points toward the existence of the asthenosphere beneath East and Southeast Asia, with heterogeneous anisotropy indicative of channel flows.

Plain Language Summary The lithospheric plates, like mosaics of the Earth's surface, are moving coherently over the weaker, convecting asthenosphere. The lithospheric structure and thickness dictated by mantle dynamics play a first-order role in understanding the active tectonics and morphological evolution of the Asian region. Here, the latest high-resolution full-waveform tomographic model, *SinoScope 1.0*, is employed to investigate the seismic structure and dynamics of the lithosphere and asthenosphere from a seismological perspective. The lithospheric thickness of known various geological units and cratonic blocks is retrieved with large variability. The observed anisotropic signatures within the lithosphere and asthenosphere provide important constraints on the deformation state and history of different tectonic provinces. The India-Eurasia collision primarily induced large-scale lithospheric deformation and thickening of the crust in the west of the North-South Gravity Lineament. The narrow low-velocity layer below the lithosphere lies beneath East and Southeast Asia and is bounded by subduction trenches and cratonic blocks, which provides seismic evidence for the low-viscosity asthenosphere that partially decouples plates from mantle flow beneath and allows plate tectonics to work above. The lithospheric thinning and extension, intensive magmatism, and mineralization are potentially associated with the strong interaction between the lithosphere and asthenospheric flow in the eastern Asian margin.

1. Introduction

The Asian region is characterized by diverse and complex patterns of extensive magmatism and intracontinental deformation, which are recorded in its geological and tectonic history and revealed by seismic imaging (Figure 1; Ma et al., 2022; Ren et al., 2013; Yin, 2010). Cenozoic (66 - 0 Ma) deformation dominates the tectonic configuration of the Asian continent along the Eastern Tethyan orogen, expressed by developments of the Tibetan Plateau and Iranian Plateau resulting from collisions of Indian and Arabian plates toward the Eurasian Plate (Chang & Zheng, 1973; DeCelles et al., 2002; Dewey, 1989; Reilinger et al., 2006). Large fragments of the Eurasian lithosphere were extruded eastward out of the central Tibetan Plateau and toward southern China and northern Indochina, significantly influencing the geological evolution of Southeast Asia (Gilder et al., 1996; Tapponnier et al., 1982, 2001). The central Asian deformation domain extends from the northern edge of the Tibetan Plateau to the northern tip of the Baikal rift system, representing one of the far-field effects of the India-Eurasia collision (Molnar & Tapponnier, 1975; Tapponnier & Molnar, 1979; Yin, 2006; Yin & Harrison, 2000). In East and Southeast Asia, subduction is the dominant plate-tectonic process, and there have been thousands of kilometers of oceanic lithosphere absorbed by the mantle beneath the Eurasian Plate during the Mesozoic (252 - 66 Ma)

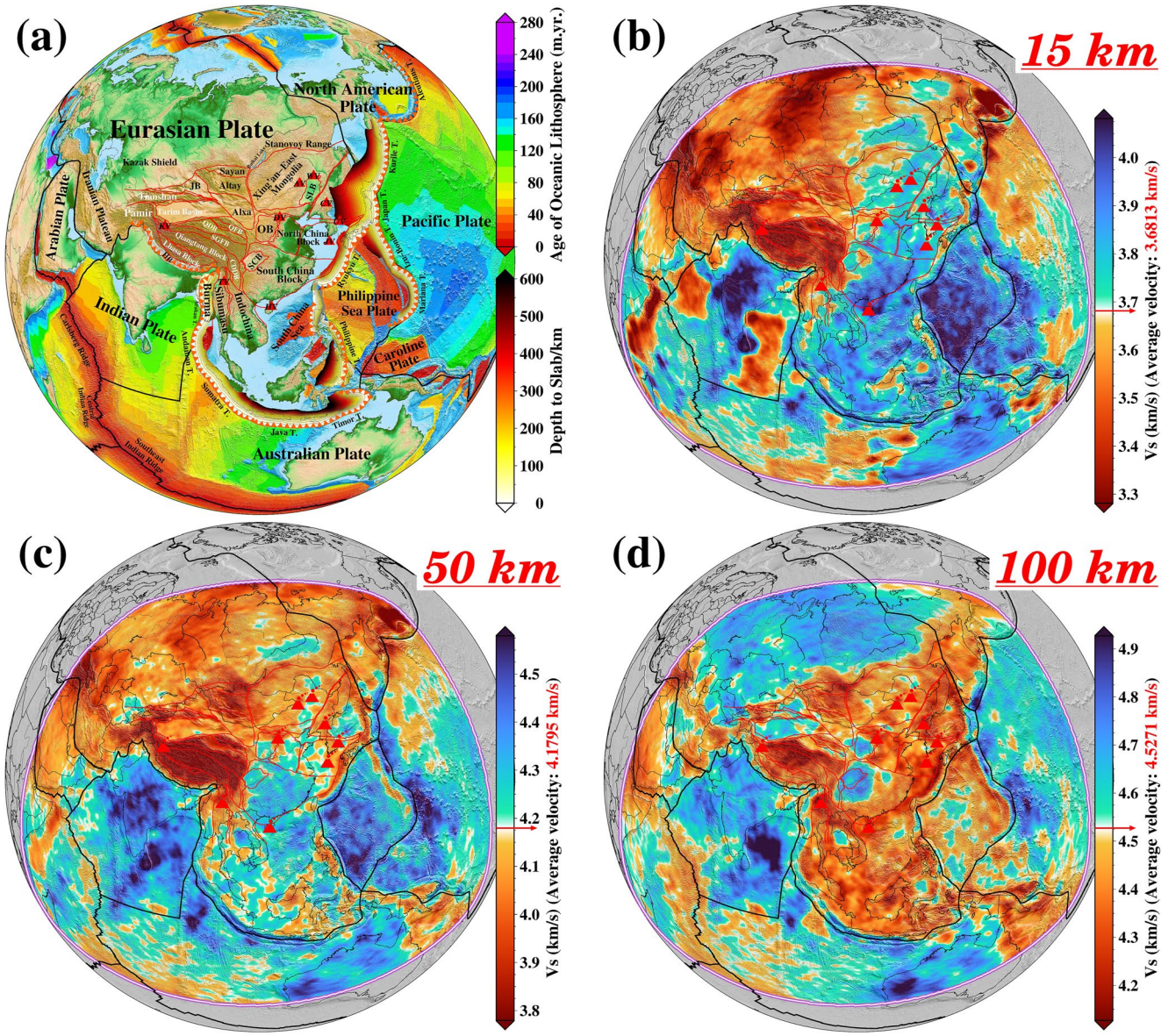

Figure 1. (a) Surface topography and major tectonic features of the broad Asian region. Colors show the age of the oceanic lithosphere with the scale shown on the top right side. Color contour lines show depths to the upper boundaries of the subducting slabs with an interval of 20 km (Slab2.0; Hayes et al., 2018), whose scale is shown on the lower right side. Black lines denote the major plate boundaries (modified from Bird, 2003), and red lines delineate main tectonic units, basins, and large fault zones. Red triangles mark the Cenozoic intraplate volcanoes. AV, Arxan Volcano; CDDB, Chuan-Dian Diamond Block; CV, Changbai Volcano; DV, Datong Volcano; HB, Himalaya Block; HV, Hainan Volcano; JB, Junggar Basin; JV, Jeju Volcano; KV, Kunlun Volcano; OB, Ordos Basin; QDB, Qaidam Basin; QFB, Qilian Fold Belt; SCB, Sichuan Basin; SGFB, Songpan Ganzi Fold Belt; SLB, Songliao Basin; TV, Tengchong Volcano; UV, Ulleung Volcano; WV, Wudalianchi Volcano. (b)–(d) Map views of the absolute isotropic shear-wave velocity at depths of 15 km, 50 km, and 100 km (Ma et al., 2022).

as the Tethys Oceans and Izanagi Plate were subducted (Müller et al., 2016). Moreover, during the Cenozoic, the Australian Plate moved northwards, the Pacific Plate and Philippine Sea Plate moved westwards, and some fragments sourced from them were collaged to Southeast Asia (Hall & Spakman, 2015; Seton et al., 2012). The interactions of these lithospheric plates are suggested to be a mechanism to cause the lithospheric thinning and destruction, intensive intraplate seismic and volcanic activities, marginal basins and volcanic arcs, and possibly the further development of the trench-arc-back-arc extensional system in the eastern Asian margin (Schellart & Lister, 2005; Zhao, 2021). To better understand how tectonic stresses of the overlying plate control asthenospheric deformation which in turn affects plate dynamics, it is necessary to study the detailed structure of the lithosphere and asthenosphere as well as the plate tectonics and mantle dynamics of the Asian region.

Cenozoic deformation of the Asian lithosphere is commonly attributed to the combined effects of continental collision and oceanic subduction. How the two classes of plate boundary processes interact with one another in controlling the widely distributed intracontinental deformation over a 3,000-km region remains the subject of debate and controversy. When collision and subduction are considered as two relatively independent processes, one thought is that the timing, location, and style of Cenozoic extensional features along the eastern margin of the Eurasian Plate are closely related to the subduction of oceanic plates rather than far-field effects of the India-Eurasia collision (e.g., Hall, 2002; Northrup et al., 1995; Royden et al., 2008; Yin, 2000). Alternatively, the India-Eurasia collision provokes compressional stresses that diverge from the collision zone and transmit through the rigid lithosphere all the way to subduction trenches, where it follows the retreat of subducting lithospheres, controlling the geometry and kinematics of major strike-slip faults and back-arc basins under the influence of the large-scale deformation of the Asian lithosphere (e.g., Jolivet et al., 1994; Tapponnier et al., 1982). Moreover, the tectonic development of the broad Asian region, commonly interpreted as a result of the plate boundary processes as discussed above, intrinsically correlates with the thermal structure of the lithosphere induced by crustal and mantle processes (e.g., Beaumont et al., 2001; Harrison et al., 1998; Jolivet et al., 2018; Molnar et al., 1993). Until now, it remains poorly understood what roles of collision and subduction coupled with time-dependent mantle flows have played in shaping the overall tectonics and deformation history of the Asian lithosphere.

In this study, our primary focus is on deciphering the seismic structure and dynamics of the lithosphere and asthenosphere beneath China and adjacent regions with the help of the latest full-waveform tomographic model of this region by Ma et al. (2022). The present work sheds important new light on the dynamic characteristics of the different tectonic provinces, the morphology of the underthrusting Indian lithosphere and its geodynamic implications, and the interaction between the lithosphere and asthenosphere in the eastern Asian margin.

2. Data and Full-Waveform Inversion

Our dataset contains more than 500,000 three-component seismograms recorded at 2,427 seismometers, corresponding to 410 earthquakes that occurred between 2009 and 2018 along the tectonically active zones of continental collision and oceanic subduction (Figure S1 in the Supporting Information S1). Physical properties of the Earth's interior are indirectly detected through seismic waves excited by earthquakes. When seismic waves propagate inside the Earth and encounter structural heterogeneities with a certain scale, wave propagation speed changes, reflection and scattering phenomena occur, and interconversions between compressional and shear waves happen. The combined effect of multiple heterogeneities produces a complicated wavefield recorded in the form of three-component seismograms. The full-waveform inversion technique based on adjoint and spectral-element methods can be employed to maximally exploit the information contained in these seismic wavefield complexities to determine the fine-scale structural heterogeneities from which they originated across various orders of magnitude in frequency and wavelength (e.g., Fichtner, 2011; Kennett & Fichtner, 2020; Tromp, 2020). Here we provide a detailed tectonic interpretation of the latest full-waveform inversion applied to the broad Asian region (*SinoScope 1.0*; Ma et al., 2022), with a special focus on China and adjacent regions where particularly dense data coverage is available. The multi-scale full-waveform inversion naturally combines the advantages of surface- and body-waves and jointly inverts for the crust and mantle structure in the period range of 30–120 s, yielding constraints on lithosphere and asthenosphere whose interactions shape the nature of plate tectonics.

3. Results and Discussion

The model parameters involved in the inversion include the wave velocities of vertically and horizontally propagating/polarized P- and S-waves (v_{pv}, v_{ph}, v_{sv}, and v_{sh}) and mass density (ρ). The data that enter the inversion process is mostly sensitive to variations in v_{sv} and v_{sh}; sensitivity kernels with respect to v_{pv}, v_{ph}, and ρ are small or negligible (Ma et al., 2022), which are not used to facilitate the interpretation of tomographic images in the following sections. Radial anisotropy is a type of transverse isotropy with a radial symmetry axis, which produces differences in propagation speed between horizontally and vertically polarized shear waves, irrespective of their propagation azimuth (e.g., Hess, 1964; Montagner & Tanimoto, 1991). The radial anisotropy parameter $\xi = (v_{sh} - v_{sv})/v_s$ provides an important indicator of lithospheric deformation in the crust and mantle or mantle flow in the asthenosphere in either horizontal direction (positive ξ) or vertical direction (negative ξ), where the isotropic shear-wave velocity is computed from v_{sh} and v_{sv} as $v_s = \sqrt{\frac{(2v_{sv}^2+v_{sh}^2)}{3}}$ (Panning & Romanowicz, 2006). Horizontal slices through the variations of v_s, v_{sv}, v_{sh} and ξ are shown in Figures S2–S12 in the Supporting Information S1.

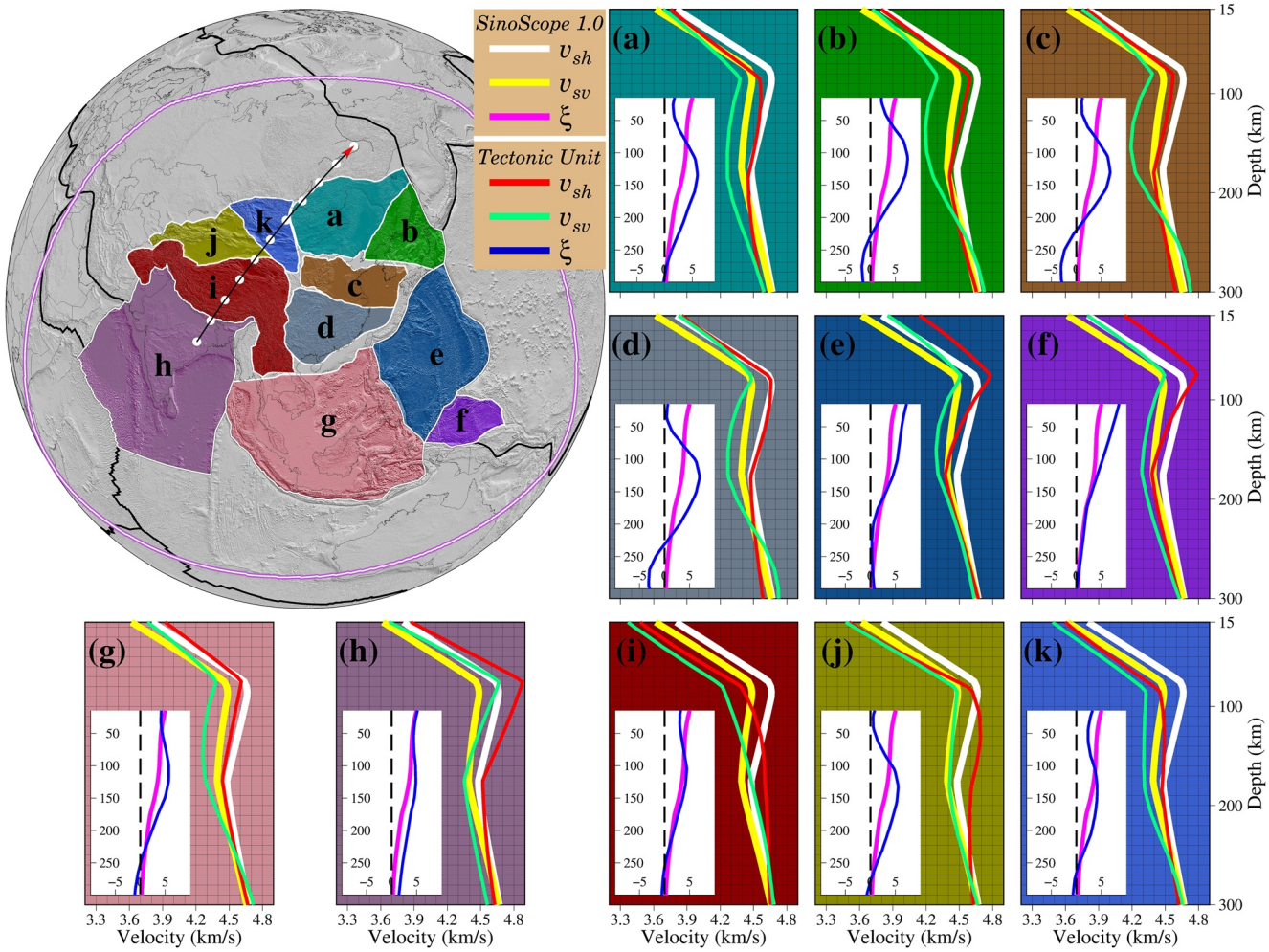

Figure 2. Topographic map shows the geographic locations of the samples and the cross-section (black line with white dots) for which the vertical profile is shown in Figures 3a–3d. Lateral averages for vertically/horizontally polarized shear-wave velocity (v_{sv} and v_{sh}) and radial shear-wave anisotropy (ξ) of 11 tectonically distinct provinces, corresponding to the color-matched shaded areas as shown in the map, which are extracted from *SinoScope 1.0* (Ma et al., 2022) and illustrated by red (v_{sh}), green (v_{sv}), and blue (ξ) lines. Bold white (v_{sh}), yellow (v_{sv}), and magenta (ξ) lines are overall 1-D radial profiles of *SinoScope 1.0* (Ma et al., 2022) and are plotted for comparison with specific tectonic units. Dashed lines represent depth profiles for isotropic models with $\xi = 0$.

3.1. Average Radial Characteristics of Different Tectonic Provinces

The tectonic framework of Asia is characterized by the assembly of diverse tectonic units along with orogenic belts in the triangular area where the Paleo-Asian Ocean, Tethyan, and Western-Pacific domains meet. To obtain more detailed characteristics of velocity and anisotropy variations with depth in the specific region, the study area is subdivided into 11 representative tectonically distinct subregions according to the distribution of major boundaries and faults (Figures 1 and 2; Bird, 2003; P. Zhang et al., 2003). The radially averaged v_{sv} and v_{sh} of the inversion domain are marked by a pronounced negative velocity gradient at depths ranging from 80 to 180 km (Figure 2). Within the upper 200 km of the Earth, variations in the radial anisotropy range between 1% and 5%, which indicates that the Asian lithosphere as a whole is dominated by horizontal movements, as derived from GPS observations (Hao et al., 2019; Wang & Shen, 2020).

The concept of asthenosphere boundary (LAB) remains debated because of different definitions based on different geophysical observations (Eaton et al., 2009). In seismic tomography, the LAB inferred from the shear-velocity structure can be defined as a sharp boundary between the high-velocity lid and the low-velocity zone, which is interpreted as the maximum of the velocity gradient ($-\delta V/\delta z$) above the low-velocity zone (Burgos et al., 2014). However, the maximum gradient is not unequivocally observed beneath the continental lithosphere due to the nonexistence of sharp velocity contrast across the LAB. The strong 3-D velocity heterogeneities of the

full-waveform tomographic model may also make some empirical approaches (e.g., Priestley & MKenzie, 2006) no longer applicable for estimating the depth of the LAB (hereafter referred to as the lithospheric thickness) for a given isotherm when converting shear-wave velocities to temperatures. It mainly stems from the possibility of unrealistic temperature values during the velocity-to-temperature conversion. Hence, we adopt the perturbation cutoff of v_{sv} and v_{sh} (δv_{sv} and $\delta v_{sh} \geq 1.25\%$ in Figures S13 and S14 in the Supporting Information S1; Maurya et al., 2016) to estimate the lithospheric thickness coupled with depth slices of the absolute shear-velocity structure down to 250 km depth (Figures S2–S12 in the Supporting Information S1) and further discuss specific structural features of major geological units in the study area.

The observations that emerge from our tomographic results reveal a thick cratonic lithosphere (~80 km; Figures S2–S5 and S13 in the Supporting Information S1 in South China, whereas the lithosphere with the presence of ≥1.25% high-velocity is just ~65 km in Northeast and North China. The thickest lithospheric keels (200–250 km) comprising deep cratonic roots are observed in the Sichuan, Ordos, and Tarim basins. The deep part of the cratonic root of the Sichuan Basin appears larger than its surface expression and extends eastward to the middle of the South China Block (Figures S13 and S14 in Supporting Information S1). The lithospheric thickness of the Indian Plate is retrieved with large variability between 150 and 250 km. Compared with the continental lithosphere, the oceanic lithosphere beneath the South China Sea, Philippine Sea Plate, and Caroline Plate is almost flatter and thinner (~90 km), overlying the low-velocity asthenosphere (Figures S2-S6 and S13-S14 in Supporting Information S1). The low-velocity zone is widely observed beneath Eastern Mongolia, Northeast, North and South China, Japan Sea, Philippine Sea Plate, Caroline Plate, Southeast Asia, and Indian Plate, except in areas of the thick continental crust where there is no apparent velocity contrast, for instance, Tibetan Plateau and Mongolian Plateau. As is evident from Figure 2, the velocity reduction pattern and depth above which reduction occurs, strongly vary with the choice of the tectonic province, reflecting their respective distinct seismic characteristics. Following a drop in v_{sv} and v_{sh}, the base of the low-velocity zone is marked by an increase: the transition is sharp in v_{sh} but gradual in v_{sv}, the Indian Plate being the only exception as both v_{sv} and v_{sh} increase sharply.

Seismic anisotropy in the upper mantle is generally attributed to the coherent lattice-preferred orientation of intrinsically anisotropic crystals such as olivine (Nicolas & Christensen, 1987; S. Zhang & Karato, 1995) and is related to past and present geodynamic processes, which provides insights into our understanding of lithospheric evolution, physical interaction between lithosphere and asthenosphere, and channel flow within the asthenosphere. Unresolved sub-wavelength heterogeneities are also capable of producing apparent anisotropy, which does not need to be related in the same way as intrinsic anisotropy (Fichtner et al., 2013). Since it is currently impossible to quantitatively separate the intrinsic and apparent anisotropy, we here restrict attention to holistic anisotropic signatures of different tectonic provinces. The strength and nature of seismic anisotropy vary significantly depending on the depth extent and tectonic unit (Figure 2). For the Philippine Sea and Caroline plates, we observe significant positive radial anisotropy ($\xi \geqslant 5$) at depths shallower than 110 km, peaking near the surface with rapidly decreasing strength at greater depths, which indicates a strong correlation with the present-day horizontal plate motion (Wu et al., 2016). The Indian Plate and Southeast Asia, which are composed of oceanic and continental lithosphere, exhibit different behavior of radial anisotropy in contrast to the Philippine Sea and Caroline plates. Southeast Asia is characterized by more substantial positive anisotropy than the average 1-D radial one down to ~200 km with the maximum value at a depth of ~120 km, whereas the pattern switches to negative at depths greater than 250 km, consistent with what Wehner et al. (2022) revealed. Beneath the Indian Plate, variations in radial anisotropy show a systematic tendency of being positive, with a secondary peak found at a depth of ~120 km except for the surface, which is the expected result of the dominant horizontal movement of the Indian Plate since the late Mesozoic. South China Block, as the relatively stable continental area, displays small to zero positive radial anisotropy in the uppermost 50 km. After that, the magnitude of radial anisotropy substantially increases and reaches a peak at a depth of ~120 km, followed by a consistent decrease at larger depths; the prominent negative pattern of radial anisotropy is observed in the depth range of ~230–300 km. The behavior of radial anisotropy beneath Eastern Mongolia, Northeast China, North China Block, and Japan Sea is similar to that of the South China Block, apart from the magnitude. The frozen-in lithospheric anisotropy ($\xi > 0$) that reflects the fossil strain field, results from a long and complex history involved in surficial tectonics (Savage, 1999), where the horizontal deformation process dominates. The existence of positive large-scale radial anisotropy with maximum values around depths of 120 km coincides with the depth range of the hypothetical shear zone between the lithosphere and asthenosphere (Ribe, 1989). Negative radial anisotropy at depths greater than 200 km largely correlates with the hot upwellings or cold downwellings above the flat slab beneath North-

east China, Japan Sea, North and South China blocks, and Southeast Asia (e.g., Ma et al., 2019; Zhao, 2021). As the far-field deformation response to the India-Eurasia collision, the low-velocity lithosphere is dominated by positive radial anisotropy beneath the Tibetan Plateau, Tianshan Orogen, eastern and western Himalayan syntaxes, and Altay-Sayan Mountain Range, which provides a good indicator of the relative horizontal movement of continental blocks in the extreme tectonic deformation environment.

3.2. Lithospheric Dynamics in Response to the India-Eurasia Collision

Since the Early Cenozoic onset of collision, the Asian lithosphere has been significantly deforming across a vast region, especially from the Himalayan Orogen in the south to the Baikal rift zone in the north (Yin, 2010).

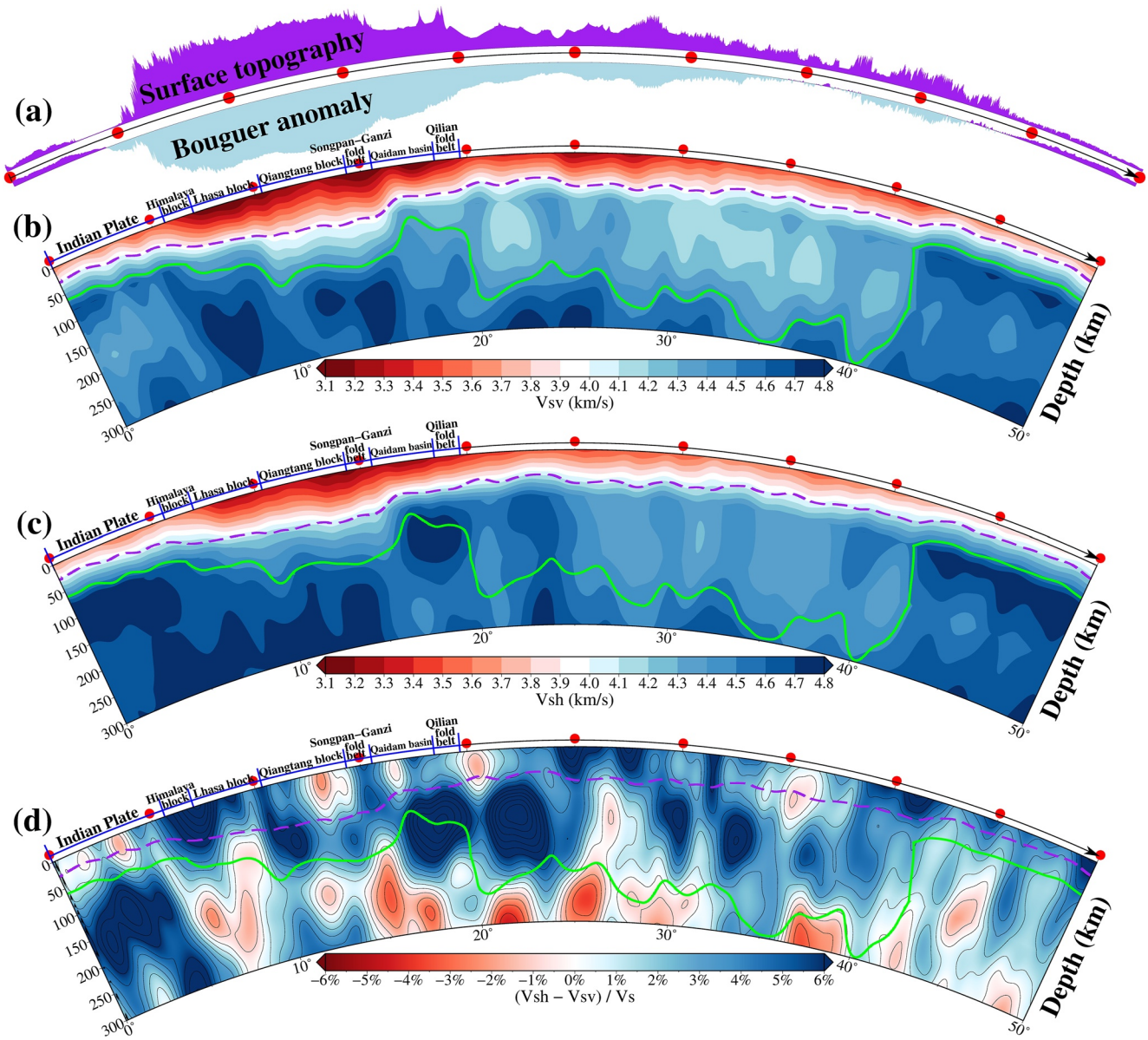

Figure 3. (a) Surface topography (top) and Bouguer gravity anomaly (bottom) from the WGM2012 model (Bonvalot et al., 2012) along the oblique profile shown in Figure 2. Purple and light blue colors denote positive and negative values of the elevation and Bouguer anomaly, respectively. (b)–(d) Cross-sections are shown for absolute vertically/horizontally polarized shear-wave velocity (v_{sv} and v_{sh}) and radial shear-wave anisotropy (ξ). Dashed magenta lines indicate the Moho depth estimated from *SinoScope 1.0* (v_s = 4.0 km/s iso-velocity to be a representation of the Moho depth; Ma et al., 2022). Green lines (indicated by an iso-velocity contour of v_s = 4.5 km/s) envelope low-velocity bodies in the mantle beneath the lithosphere. Red dots on the frame of each cross-section are marked every 5°.

The India-Eurasia convergence has driven Himalayan mountain building, Tibetan Plateau formation, and widespread deformation outside the collision zone, accommodating north-south crustal shortening with estimates in the range from a few hundred kilometres to >2,000 km (e.g., Huang et al., 2015; Li et al., 2015; Tapponnier et al., 2001). The most prominent features of the Tibetan Plateau and its surrounding deforming area are the thicker crust (50–90 km) than typical continental crust and the strongest negative Bouguer gravity anomaly (up to −500 mGal) in the world (Figure S15 in Supporting Information S1). The cross-section through the Tibetan Plateau shows that the Moho (the boundary between the crust and mantle) deepens gently northward from ∼35 km beneath the Tethyan Himalaya to 75–90 km beneath the Qiangtang Block and Songpan Ganzi Fold Belt (Figure 3), consistent with the results of receiver function analysis (e.g., Cheng et al., 2021; He et al., 2014). The Indian lithosphere is underthrusting beneath the Himalaya along the Main Himalayan Thrust and continues to extend beneath the Lhasa and Qiangtang blocks with ramp-flat geometry (Figures S16-S21 in Supporting Information S1), which has contributed to the crustal thickening, resulting in the deep Moho there (Figure 3). The asthenosphere carrying the northward movement of the Indian lithospheric mantle exhibits significant positive radial anisotropy ($\xi > 5$) along the strike. As the tectonic transitional zone between the Tibetan Plateau and stable Siberian Craton, the widely distributed deformation range from the Qilian Fold Belt to the Baikal rift zone is underlain by relatively low-velocity mantle with dominant positive radial anisotropy. It probably reconciles with compressional stresses that diverge from the collision zone. In Figure 3, there exists a good agreement between the underthrusting Indian lithosphere and the low Bouguer anomaly along the N–S trending profile, indicating that the geometry of the Bouguer gravity low is induced by the crustal thickening beneath the Tibetan Plateau. Across the well-known North-South Gravity Lineament (NSGL) extending >4,000 km from Siberia to South China, there is an abrupt shift in the Moho topography and Bouguer gravity anomaly (Figures S22–S26 in Supporting Information S1). The NSGL is likely caused primarily by variations in the Moho depth as a result of the post-collision crustal thickening in the west of the NSGL. The different lithospheric compositions on either side of the NSGL probably contribute secondarily to the formation of the NSGL, which is most likely related to the interaction between the lithosphere and asthenosphere beneath East and Southeast Asia.

3.3. Asthenosphere Beneath East and Southeast Asia

The seismic low-velocity channels imaged beneath the East and Southeast Asian lithosphere reflect the presence of the low-viscosity asthenosphere (Figure 4), which has weaker mechanical strength than the overlying lithosphere and decouples tectonic plates from the deep mantle. The widespread and prominent low-velocity asthenosphere with a thickness range of ∼100–300 km is bounded by the subducting slab along the strongly curved convergent boundary (Kurile, Japan, Ryukyu, Philippine, Timor, Java, Sumatra, Andaman, and Arakan) and lithospheric keels (Sichuan and Ordos blocks), which is also coincident spatially with extensive intraplate volcanism. The presence of apparent radial anisotropy ($\xi > 4$) in the asthenosphere reflects strong shear flow beneath the lithosphere, which is accompanied by the largest shear strain at the top and bottom boundaries of the flow channel (Figure 4c). The heating from the asthenosphere on the lithosphere subsequently triggered extensive magmatism, mineralization, intraplate volcanism, and the widespread development of extensional structures, and the relative shear motion between the lithosphere and asthenosphere could induce the complex configuration of the lithosphere through extreme lithospheric thinning in the eastern Asian margin (e.g., Yang et al., 2021; Zheng et al., 2018). Beneath the asthenosphere, strong negative radial anisotropy areas indicate vertically oriented structures that can be assigned to specific tectonic events, for example, cold downwellings (subducting slabs, detached lithosphere removed by the shear asthenospheric flows, etc.) along active continental margins (e.g., K.-J. Zhang, 2012; Ma et al., 2019).

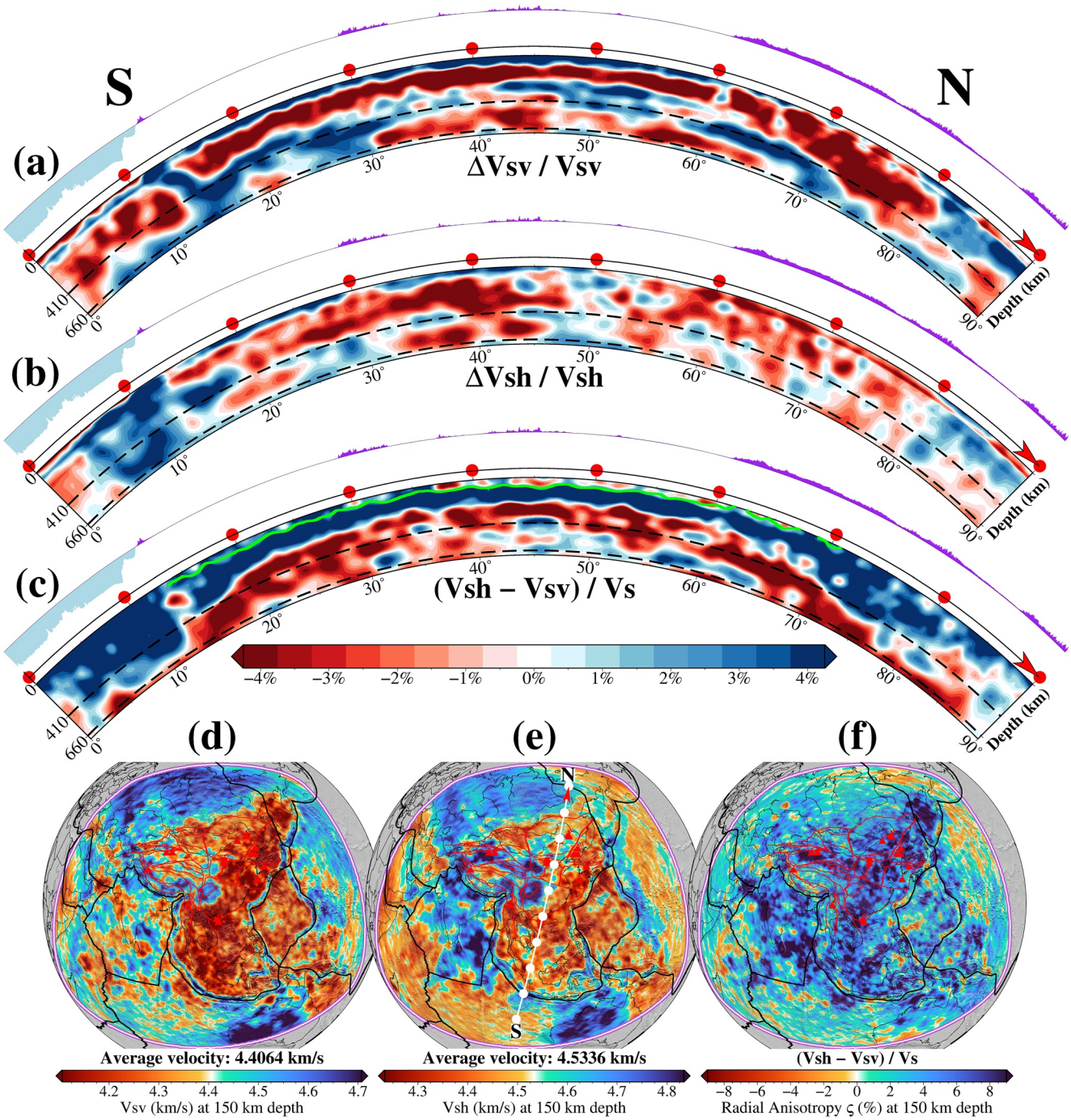

Figure 4. (a)–(c) North-south cross-sections of vertically/horizontally polarized shear-wave velocity (v_{sv} and v_{sh}) perturbations and radial shear-wave anisotropy (ξ) along the profile shown in the map (e). Surface topography and bathymetry along each profile is shown on the top of each cross-section. Dashed black lines denote the 410-km and 660-km discontinuities; Red dots on the frame of each cross-section are marked every 10°. The green line denotes the estimated LAB. (d)–(f) Distributions of the absolute v_{sv} and v_{sh}, and ξ at 150 km depth; their scales are shown at the bottom. Red triangles mark the Cenozoic intraplate volcanoes.

4. Conclusions

This study provides new information on the radially anisotropic signature and dynamics of the lithosphere and asthenosphere utilizing high-resolution full-waveform tomographic images in the Asian region, which is intended to improve our quantitative understanding of the regional tectonic evolution. The large-scale lithospheric deformation in the west of the NSGL characterized by particularly low seismic velocities is dominated by strong

radial anisotropy with enhanced SH-wave speed and crustal thickening, potentially reflecting prominent shear strain caused by compressional stresses that diverge from the India-Eurasia collision zone toward the stable Siberian Craton. The underthrusting Indian lithosphere has reached the Songpan Ganzi Fold Belt with a ramp-flat shape, down to ~250–300 km. Lithospheric keels (Sichuan, Ordos, and Tarim basins) comprise deep cratonic roots (~200–250 km), which encircle the northwest and east borders of the Tibetan Plateau and might play an important role in the internal deformation and tectonic escape of lithosphere in the Tibetan Plateau. In East and Southeast Asia, the lithospheric thickness exhibits large variations underneath different tectonic units, and the presence of lamellar-like positive radial anisotropy within the asthenosphere indicates the asthenospheric flow field is dominated by horizontal movements. The lithospheric thinning and extension, magmatism, mineralization, and intraplate volcanism are probably related to the strong interaction between the lithosphere and asthenosphere in the eastern Asian margin.

Data Availability Statement

Data are available through Ma et al. (2022).

Acknowledgments
J. Ma acknowledges the financial support from the China Scholarship Council. S.-J. Chang was supported by the Korea Meteorological Administration Research and Development Program under Grant KMI 2022-00810, by the National Research Foundation of Korea (NRF) grant funded by the Korean government (MSIT) (2019R1A2C208506111), and by Basic Science Research Program through the NRF funded by the Ministry of Education (2019R1A6A1A03033167). Y. Tian was supported by the grant from the National Natural Science Foundation of China (41874049 and 42274065). The authors are very grateful to Lucy Flesch (the Editor), Deborah Wehner, and an anonymous reviewer for their constructive comments and suggestions that improved the manuscript. Open Access funding enabled and organized by Projekt DEAL.

References

Beaumont, C., Jamieson, R. A., Nguyen, M., & Lee, B. (2001). Himalayan tectonics explained by extrusion of a low-viscosity crustal channel coupled to focused surface denudation. *Nature*, *414*(6865), 738–742.

Bird, P. (2003). An updated digital model of plate boundaries. *Geochemistry, Geophysics, Geosystems*, *4*(3). https://doi.org/10.1029/2001GC000252

Bonvalot, S., Balmino, G., Briais, A., Kuhn, M., Peyrefitte, A., Vales, N., et al. (2012). *World gravity map*. Commission for the Geological Map of the World.

Burgos, G., Montagner, J.-P., Beucler, E., Capdeville, Y., Mocquet, A., & Drilleau, M. (2014). Oceanic lithosphere-asthenosphere boundary from surface wave dispersion data. *Journal of Geophysical Research: Solid Earth*, *119*(2), 1079–1093. https://doi.org/10.1002/2013JB010528

Chang, C.-F., & Zheng, X.-L. (1973). Tectonic features of the Mount Jolmo Lungma region in southern Tibet, China. 8(1). Retrieved from http://en.igg-journals.cn/article/id/geology_8767

Cheng, S., Xiao, X., Wu, J., Wang, W., Sun, L., Wang, X., & Wen, L. (2021). Crustal thickness and Vp/Vs variation beneath continental China revealed by receiver function analysis. *Geophysical Journal International*, *228*(3), 1731–1749. https://doi.org/10.1093/gji/ggab433

DeCelles, P. G., Robinson, D. M., & Zandt, G. (2002). Implications of shortening in the Himalayan fold-thrust belt for uplift of the Tibetan plateau. *Tectonics*, *21*(6), 12-1–21-25. https://doi.org/10.1029/2001TC001322

Dewey, J. (1989). Tectonic evolution of the India Eurasia collision zone. *Eclogae Geologicae Helvetiae*, *82*, 717–734.

Eaton, D. W., Darbyshire, F., Evans, R. L., Grütter, H., Jones, A. G., & Yuan, X. (2009). The elusive lithosphere–asthenosphere boundary (lab) beneath cratons. *Lithos*, *109*(1), 1–22. (Continental Lithospheric Mantle: The Petro-Geophysical Approach). https://doi.org/10.1016/j.lithos.2008.05.009

Fichtner, A. (2011). *Full seismic waveform modelling and inversion*. Springer. https://doi.org/10.1007/978-3-642-15807-0

Fichtner, A., Kennett, B. L., & Trampert, J. (2013). Separating intrinsic and apparent anisotropy. *Physics of the Earth and Planetary Interiors*, *219*, 11–20. https://doi.org/10.1016/j.pepi.2013.03.006

Gilder, S. A., Gill, J., Coe, R. S., Zhao, X., Liu, Z., Wang, G., et al. (1996). Isotopic and paleomagnetic constraints on the mesozoic tectonic evolution of south China. *Journal of Geophysical Research: Solid Earth*, *101*(B7), 16137–16154. https://doi.org/10.1029/96JB00662

Hall, R. (2002). Cenozoic geological and plate tectonic evolution of se Asia and the SW Pacific: Computer-based reconstructions, model and animations. *Journal of Asian Earth Sciences*, *20*(4), 353–431.

Hall, R., & Spakman, W. (2015). Mantle structure and tectonic history of SE Asia. *Tectonophysics*, *658*, 14–45. https://doi.org/10.1016/j.tecto.2015.07.003

Hao, M., Li, Y., & Zhuang, W. (2019). Crustal movement and strain distribution in East Asia revealed by GPS observations. *Scientific Reports*, *9*(1), 1–11.

Harrison, T. M., Grove, M., Lovera, O. M., & Catlos, E. (1998). A model for the origin of himalayan anatexis and inverted metamorphism. *Journal of Geophysical Research: Solid Earth*, *103*(B11), 27017–27032.

Hayes, G. P., Moore, G. L., Portner, D. E., Hearne, M., Flamme, H., Furtney, M., & Smoczyk, G. M. (2018). Slab2, a comprehensive subduction zone geometry model. *Science*, *362*(6410), 58–61.

He, R., Shang, X., Yu, C., Zhang, H., & Van der Hilst, R. D. (2014). A unified map of Moho depth and Vp/Vs ratio of continental China by receiver function analysis. *Geophysical Journal International*, *199*(3), 1910–1918. https://doi.org/10.1093/gji/ggu365

Hess, H. H. (1964). Seismic anisotropy of the uppermost mantle under oceans. *Nature*, *203*(4945), 629–631. https://doi.org/10.1038/203629a0

Huang, W., van Hinsbergen, D. J. J., Lippert, P. C., Guo, Z., & Dupont-Nivet, G. (2015). Paleomagnetic tests of tectonic reconstructions of the India-Asia collision zone. *Geophysical Research Letters*, *42*(8), 2642–2649. https://doi.org/10.1002/2015GL063749

Jolivet, L., Faccenna, C., Becker, T., Tesauro, M., Sternai, P., & Bouilhol, P. (2018). Mantle flow and deforming continents: From India-Asia convergence to Pacific subduction. *Tectonics*, *37*(9), 2887–2914. https://doi.org/10.1029/2018TC005036

Jolivet, L., Tamaki, K., & Fournier, M. (1994). Japan sea, opening history and mechanism: A synthesis. *Journal of Geophysical Research: Solid Earth*, *99*(B11), 22237–22259.

Kennett, B. L. N., & Fichtner, A. (2020). *Exploiting seismic waveforms: Correlation, heterogeneity and inversion*. Cambridge University Press. https://doi.org/10.1017/9781108903035

Li, Y., Wang, C., Dai, J., Xu, G., Hou, Y., & Li, X. (2015). Propagation of the deformation and growth of the Tibetan–Himalayan orogen: A review. *Earth-Science Reviews*, *143*, 36–61. https://doi.org/10.1016/j.earscirev.2015.01.001

Ma, J., Bunge, H.-P., Thrastarson, S., Fichtner, A., Herwaarden, D.-P. v., Tian, Y., et al. (2022). Seismic full-waveform inversion of the crust-mantle structure beneath China and adjacent regions. *Journal of Geophysical Research: Solid Earth*, *127*(9), e2022JB024957. https://doi.org/10.1029/2022JB024957

Ma, J., Tian, Y., Zhao, D., Liu, C., & Liu, T. (2019). Mantle dynamics of Western Pacific and East Asia: New insights from p wave anisotropic tomography. *Geochemistry, Geophysics, Geosystems*, *20*(7), 3628–3658. https://doi.org/10.1029/2019GC008373

Maurya, S., Montagner, J.-P., Kumar, M. R., Stutzmann, E., Kiselev, S., Burgos, G., et al. (2016). Imaging the lithospheric structure beneath the Indian continent. *Journal of Geophysical Research: Solid Earth*, *121*(10), 7450–7468. https://doi.org/10.1002/2016JB012948

Molnar, P., England, P., & Martinod, J. (1993). Mantle dynamics, uplift of the Tibetan Plateau, and the Indian monsoon. *Reviews of Geophysics*, *31*(4), 357–396.

Molnar, P., & Tapponnier, P. (1975). Cenozoic tectonics of Asia: Effects of a continental collision: Features of recent continental tectonics in Asia can be interpreted as results of the India-Eurasia collision. *Science*, *189*(4201), 419–426.

Montagner, J.-P., & Tanimoto, T. (1991). Global upper mantle tomography of seismic velocities and anisotropies. *Journal of Geophysical Research: Solid Earth*, *96*(B12), 20337–20351. https://doi.org/10.1029/91jb01890

Müller, R. D., Seton, M., Zahirovic, S., Williams, S. E., Matthews, K. J., Wright, N. M., et al. (2016). Ocean basin evolution and global-scale plate reorganization events since pangea breakup. *Annual Review of Earth and Planetary Sciences*, *44*(1), 107–138. https://doi.org/10.1146/annurev-earth-060115-012211

Nicolas, A., & Christensen, N. I. (1987). Formation of anisotropy in upper mantle peridotites - A review. In *Composition, structure and dynamics of the lithosphere?asthenosphere system* (pp. 111–123). American Geophysical Union (AGU). https://doi.org/10.1029/GD016p0111

Northrup, C., Royden, L., & Burchfiel, B. (1995). Motion of the Pacific plate relative to Eurasia and its potential relation to cenozoic extension along the eastern margin of Eurasia. *Geology*, *23*(8), 719–722.

Panning, M., & Romanowicz, B. (2006). A three-dimensional radially anisotropic model of shear velocity in the whole mantle. *Geophysical Journal International*, *167*(1), 361–379. https://doi.org/10.1111/j.1365-246x.2006.03100.x

Priestley, K., & Mkenzie, D. (2006). The thermal structure of the lithosphere from shear wave velocities. *Earth and Planetary Science Letters*, *244*(1), 285–301. https://doi.org/10.1016/j.epsl.2006.01.008

Reilinger, R., McClusky, S., Vernant, P., Lawrence, S., Ergintav, S., Cakmak, R., et al. (2006). GPS constraints on continental deformation in the africa-arabia-eurasia continental collision zone and implications for the dynamics of plate interactions. *Journal of Geophysical Research*, *111*(B5). 10.1029/2005JB004051

Ren, J., Niu, B., Wang, J., Jin, X., Zhao, L., & Liu, R. (2013). Advances in research of Asian geology—A summary of 1:5m international geological map of Asia project. *Journal of Asian Earth Sciences*, *72*, 3–11. (Geological Evolution of Asia) https://doi.org/10.1016/j.jseaes.2013.02.006

Ribe, N. M. (1989). Seismic anisotropy and mantle flow. *Journal of Geophysical Research*, *94*(B4), 4213–4223. https://doi.org/10.1029/JB094iB04p04213

Royden, L. H., Burchfiel, B. C., & van der Hilst, R. D. (2008). The geological evolution of the Tibetan plateau. *Science*, *321*(5892), 1054–1058.

Savage, M. K. (1999). Seismic anisotropy and mantle deformation: What have we learned from shear wave splitting? *Reviews of Geophysics*, *37*(1), 65–106. https://doi.org/10.1029/98rg02075

Schellart, W. P., & Lister, G. (2005). The role of the east Asian active margin in widespread extensional and strike-slip deformation in East Asia. *Journal of the Geological Society*, *162*(6), 959–972.

Seton, M., Müller, R., Zahirovic, S., Gaina, C., Torsvik, T., Shephard, G., et al. (2012). Global continental and ocean basin reconstructions since 200ma. *Earth-Science Reviews*, *113*(3), 212–270. https://doi.org/10.1016/j.earscirev.2012.03.002

Tapponnier, P., & Molnar, P. (1979). Active faulting and cenozoic tectonics of the Tien Shan, Mongolia, and Baikal regions. *Journal of Geophysical Research*, *84*(B7), 3425–3459.

Tapponnier, P., Peltzer, G., Le Dain, A. Y., Armijo, R., & Cobbold, P. (1982). Propagating extrusion tectonics in Asia: New insights from simple experiments with plasticine. *Geology*, *10*(12), 611–616. https://doi.org/10.1130/0091-7613(1982)10<611:PETIAN>2.0

Tapponnier, P., Xu, Z., Roger, F., Meyer, B., Arnaud, N., Wittlinger, G., & Jingsui, Y. (2001). Oblique stepwise rise and growth of the Tibet plateau. *Science*, *294*(5547), 1671–1677.

Tromp, J. (2020). Seismic wavefield imaging of earth's interior across scales. *Nature Reviews Earth & Environment*, *1*(1), 40–53.

Wang, M., & Shen, Z.-K. (2020). Present-day crustal deformation of continental China derived from GPS and its tectonic implications. *Journal of Geophysical Research: Solid Earth*, *125*(2), e2019JB018774. https://doi.org/10.1029/2019JB018774

Wehner, D., Blom, N., Rawlinson, N., Daryono Böhm, C., Miller, M. S., Supendi, P., & Widiyantoro, S. (2022). Sassy21: A 3-d seismic structural model of the lithosphere and underlying mantle beneath southeast Asia from multi-scale adjoint waveform tomography. *Journal of Geophysical Research: Solid Earth*, *127*(3), e2021JB022930. https://doi.org/10.1029/2021JB022930

Wu, J., Suppe, J., Lu, R., & Kanda, R. (2016). Philippine Sea and East Asian plate tectonics since 52 Ma constrained by new subducted slab reconstruction methods. *Journal of Geophysical Research: Solid Earth*, *121*(6), 4670–4741. https://doi.org/10.1002/2016jb012923

Yang, J.-H., Xu, L., Sun, J.-F., Zeng, Q., Zhao, Y.-N., Wang, H., & Zhu, Y.-S. (2021). Geodynamics of decratonization and related magmatism and mineralization in the North China Craton. *Science China Earth Sciences*, *64*(9), 1409–1427.

Yin, A. (2000). Mode of cenozoic east-west extension in Tibet suggesting a common origin of rifts in Asia during the indo-Asian collision. *Journal of Geophysical Research*, *105*(B9), 21745–21759.

Yin, A. (2006). Cenozoic tectonic evolution of the Himalayan orogen as constrained by along-strike variation of structural geometry, exhumation history, and foreland sedimentation. *Earth-Science Reviews*, *76*(1–2), 1–131.

Yin, A. (2010). Cenozoic tectonic evolution of Asia: A preliminary synthesis. *Tectonophysics*, *488*(1), 293–325. (Extensional Tectonics in the Basin and Range, the Aegean, and Western Anatolia). https://doi.org/10.1016/j.tecto.2009.06.002

Yin, A., & Harrison, T. M. (2000). Geologic evolution of the himalayan-Tibetan orogen. *Annual Review of Earth and Planetary Sciences*, *28*(1), 211–280.

Zhang, K.-J. (2012). Destruction of the north China craton: Lithosphere folding-induced removal of lithospheric mantle? *Journal of Geodynamics*, *53*, 8–17. https://doi.org/10.1016/j.jog.2011.07.005

Zhang, P., Deng, Q., Zhang, G., Ma, J., Gan, W., Min, W., et al. (2003). Active tectonic blocks and strong earthquakes in the continent of China. *Science in China - Series D: Earth Sciences*, *46*(2), 13–24.

Zhang, S., & Karato, S.-I. (1995). Lattice preferred orientation of olivine aggregates deformed in simple shear. *Nature*, *375*(6534), 774–777.

Zhao, D. (2021). Seismic imaging of northwest Pacific and East Asia: New insight into volcanism, seismogenesis and geodynamics. *Earth-Science Reviews*, *214*, 103507.

Zheng, Y., Xu, Z., Zhao, Z., & Dai, L. (2018). Mesozoic mafic magmatism in north China: Implications for thinning and destruction of cratonic lithosphere. *Science China Earth Sciences*, *61*(4), 353–385.